Danish Meteorological Institute
Ministry of Climate and Energy

Scientific Report 06-02

A short introduction to the dynamics of severe convection

Niels Woetmann Nielsen

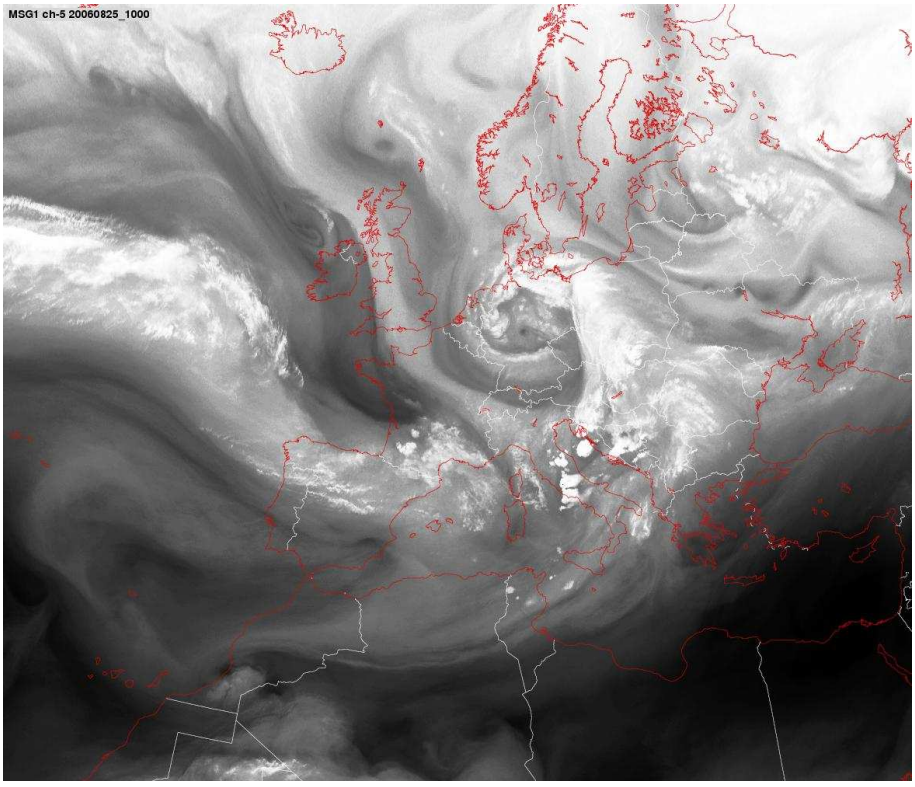

Colophone

Serial title:
Scientific Report 06-02

Title:
A short introduction to the dynamics of severe convection

Subtitle:

Authors:
Niels Woetmann Nielsen

Other Contributers:

Responsible Institution:
Danish Meteorological Institute

Language:
English

Keywords:
convection, cell, multicell, supercell, convective system, mesocyclone, updraft, downdraft, self-organization, storm splitting, right movers

Url:
www.dmi.dk/dmi/sr06-02

ISSN:
ISBN:
87-7478-535-4

Version:
1

Website:
www.dmi.dk

Dansk Resume

Tordenbyger kan under visse betingelser organisere sig i multicelle og/eller supercelle systemer. Et multicelle system opleves som et langvarigt og særdeles kraftigt tordenvejr og i nogle tilfælde er systemet istand til at skabe tornadoer. Der redegøres kort for hvordan vekselvirkning mellem baggrundsstrømning og strømning knyttet til tordenbyger kan skabe gunstige betingelser for selvorganisering. Et multicelle tordenvejrssystem, som hærgede Nordtyskland, undersøges.

Abstract

Deep convection is often triggered by forcing on synoptic to mesoscale. Once deep convection has formed, it may organize itself into a severe convective system consisting of multicells and/or supercells. Interaction between the synoptic-scale flow and the convective-scale flow plays an important role in this self-organization. The interaction generates a dynamic perturbation pressure and vertical gradients in the perturbation pressure may trigger new convective updrafts. The theory behind is briefly reviewed, and a multicell storm case over Northern Germany is investigated.

Introduction

In contrast to convection in the planetary boundary layer, severe convection usually involves the whole depth of the troposphere, with overshooting tops penetrating the lower stratosphere. The three spatial dimensions, L_x, L_y and L_z, of a severe convection cell is of the same order of magnitude ($L_x \sim L_y \sim L_z \sim 10\,km$). The acceleration of the three dimensional wind is typically $> 10^{-2}\,\mathrm{ms}^{-2}$ and since $u \sim v \sim w \sim 10\,ms^{-1}$, the Coriolis acceleration is typically of order $10^{-3}\,\mathrm{ms}^{-2}$, which means that a typical Rossby number, $Ro = |\frac{D\vec{V}}{Dt}|/f|\vec{V}|$, for severe convection is $Ro \sim 10$. This should be compared with $Ro \sim 0.1$ for 1000 km-scale extratropical cyclones.

Severe convection may develop in a moist environment with conditional or potential/convective instability. Longer lasting severe convection such as multicell or supercell storms tend to develop if the environment also has a significant vertical shear of the horizontal wind.

In the present lecture note it is shown how the environmental velocity shear is able to influence the development of new convective cells in conditions favorable for deep convection.

The frontpage image shows a Meteosat Second Generation (MSG) water vapor channel 5 image from 10 UTC on 25 August 2006. Isolated thunderstorms are seen as white spots in the image over for example Italy and the Adriatic Sea. In certain weather conditions a multi-cell system may form.

Deep convection

Ordinary deep convection

In ordinary deep convection, occurring in an environment with weak or no vertical shear of the horizontal wind, the perturbation pressure generated by convection has weak or no contribution from interaction of the wind in the environment with the wind generated by convection (the perturbation wind field). The convective updrafts tend to be vertical. The dry adiabatic cooling to saturation in the updraft initiates formation of cloud particles (i.e. water droplets and/or ice crystals). The level where cloud particles begin to form is called the lifting condensation level (LCL). This level may be above, identical with or below the level of free convection (LFC). The latter is the level where the lifted air becomes positively buoyant, i.e. warmer than the surrounding air. As the updraft, loaded with cloud particles, accelerates upward it cools moist adiabatically, while cloud particles grow in size by supply of condensed water vapor and due to cloud micro-physical processes. This stage of convection is called the *cumulus stage*. It is characterized entirely by updraft air. In the next, *mature stage*, cloud particles have become so heavy that their fall speed exceeds the updraft velocity. The negatively buoyant cloud particles initiate a downdraft. The *mature stage* is characterized by both updraft and downdraft air. Evaporation from precipitation particles, as they fall through pockets of unsaturated air above the LCL, and particularly as they fall through the unsaturated air below the LCL, cools the downdraft air making the downdraft more negatively buoyant. Without vertical shear of the wind in the environment the downdraft destroys the updraft underneath it. The stage characterized entirely by downdraft air is called the *dissipation stage*. In the cloud-relative system the cool downdraft air spreads out uniformly in all directions as it approaches the surface. It forms a gust front in the transition zone to the warmer air in the environment. The forced lifting of air at the gust front may trigger new cells more or less randomly along the gust front if the ascent is able to lift the near-surface air to the LFC of the environment. A cell is here defined as the region of precipitation associated with the updraft. Since the vertical extent and the vertical velocity in an ordinary cell is of the order of 10 km and $10\,\mathrm{m\,s}^{-1}$, respectively, the life time of a cell (i.e. from its cumulus stage to its dissipation stage) is typically between 30 and 40 minutes. Since the horizontal scale tends to be of the same order of magnitude as the vertical scale the precipitation area in the cell

is of the order $100\,\mathrm{km}^2$.

If the environment has a LCL far above the ground the enhanced evaporation of precipitation particles below the cloud base may create vigorous downdrafts and severe near-surface wind gusts behind advancing gust fronts.

Deep convection in an environment with vertical wind shear

Convection in an environment characterized by considerably vertical shear of the horizontal wind behaves differently from ordinary deep convection. There are two significant differences.

One is that the vertical shear of the wind in the environment tilts the updraft in a cell with respect to the vertical. A tilt in the inflow down-wind direction prevents the downdraft air from falling into the updraft air. The spatial separation of the updraft and downdraft air in this case creates a potential for a longer-lived cell.

The other significant difference is that the perturbation pressure generated by the interaction of the flow in the environment with the perturbation wind field of the cell creates favorable regions for growth of new cells. The latter contributes to organization of the convection into a multicell system. If the environment has substantial convective available potential energy (CAPE) and large vertical wind shear a cell may be transformed into a supercell storm with a life time of several hours.

The perturbation pressure generated by the *interaction* is given (approximately) by

$$p_L \sim 2\rho_e \left(\frac{\partial u_e}{\partial z}\frac{\partial w_p}{\partial x} + \frac{\partial v_e}{\partial z}\frac{\partial w_p}{\partial y} \right) \tag{1}$$

and

$$p_{NL} \sim -\rho_e \frac{1}{2}{\zeta_{pz}}^2, \tag{2}$$

where $\sim$ means "proportional to". In (1) p_L is the linear and in (2) p_{NL} is the nonlinear part of the perturbation pressure. Subscripts e and p mean environment and perturbation variables, respectively. For convenience, subscript p on the perturbation pressure has been omitted. The derivation of (1) and (2), partly following Blustein, 1993, is given in the Appendix.

In (2) the perturbation vorticity, ζ_{pz}, along the vertical axis is generated by the twisting term in the vorticity equation, i.e. by

$$\left(\frac{\partial \zeta_{pz}}{\partial t}\right)_{twist} = \frac{\partial u_e}{\partial z}\frac{\partial w_p}{\partial y} - \frac{\partial v_e}{\partial z}\frac{\partial w_p}{\partial x}. \tag{3}$$

According to (3) the generation of perturbation vorticity ζ_{pz} is a result of interaction between a vertically sheared environmental flow ($\partial \vec{V}_e/\partial z$) and the updraft velocity w_p. Equations (1) and (2) show that both the linear and nonlinear perturbation pressure is associated with interaction between updraft and the flow in the environment. A multicell storm system consists of a number of celles at different stages of development. In general the individual cells move in a direction different form the storm system and the environmental wind $\vec{V}_e$ is measured relative to the moving system instead of relative to the Earth.

Effect of linear perturbation pressure

In a background (environmental) flow with a unidirectional shear along the x-axis (1) simplifies to

$$p_L \sim 2\rho_e \frac{\partial u_e}{\partial z}\frac{\partial w_p}{\partial x}. \quad (4)$$

If the positive x-direction is in the downshear direction, i.e. $\partial u_e/\partial z > 0$ (Figure 1a), it follows from (4) that p_L is positive and negative on the upshear and downshear side of the updraft, respectively. As shown in Figure 1a, this means a positive and negative linear perturbation pressure on the left and right side of the updraft, when looking in the positive y-direction. The left part of Figure 1a shows a horizontal cross section through an idealized circular symmetric updraft with maximum numerical horizontal shear of the updraft ($|\partial w_p/\partial x|$) along the inner (blue) circle. The right part of the figure shows the change with height of the background wind, u_e, in case of a constant vertical shear ($\partial u_e/\partial z = c_x$). The maximum numerical perturbation shear ($|\partial w_p/\partial x|$) tends to occur at the level z_{max} of maximum updraft velocity. Since the vertical shear of u_e is constant in the figure, the maximum numerical perturbation pressure occurs at z_{max}, at the two crosses marked on the inner (blue) circle. This means, for levels below z_{max}, that the vertical perturbation pressure gradient ($\partial p_N/\partial z$) is positive on the left and negative on the right side of the updraft when looking in the positive y-direction. *The vertical linear perturbation pressure gradient force may therefore trigger development of new cells on the downshear (right) side and suppress growth of new cells on the upshear (left) side of the updraft.*

In a way the updraft can be considered as an obstacle in the background flow that generates high pressure on the windward and low pressure on the leeward side of the obstacle. In the case with $c_x > 0$ the wind speed increases with height. This is associated with an increase and a decrease with height of the perturbation pressure on the windward and leeward side, respectively. Accordingly, the high perturbation pressure on the windward side generates subsidence. Likewise, the low perturbation pressure on the leeward side generates ascent. If the wind is easterly near the surface and westerly in the upper troposphere the windward and leeward side would change accordingly. Therefore, ascent and decent occurs on the downshear and upshear side of the obstacle, respectively.

Influence of temperature advection

In cases with temperature advection in the environment the vertical shear of the wind in the environment can not be unidirectional. In a Northern Hemisphere environment with warm and cold advection the wind is veering (turning anticyclonically) and backing (turning cyclonically) with height, respectively. In Figure 1b cases are depicted with v_e (the background wind component in the y-direction) increasing (black in Figure 1b) and decreasing (red in Figure 1b) with height. The red and black v_e-profiles may represent cases with both warm and cold advection, but if for example u_e is positive and constant with height, the red and black v_e-profiles represent warm and cold advection, respectively.

According to (1) the linear perturbation pressure becomes

$$p_L \sim 2\rho_e \frac{\partial v_e}{\partial z}\frac{\partial w_p}{\partial y}. \quad (5)$$

It follows (by using similar arguments as in the discussion of Figure 1a) that the perturbation pressure p_L becomes positive and negative on the upshear and downshear side of the updraft, respectively. In terms of left and right, when looking in the positive x-direction, it is necessary to distinguish between the red and black v_e-profiles. In cases with a red profile, p_L becomes positive and negative on the left and right side of the updraft, respectively, whereas the opposite holds for the black profile. With conditions as in Figure 1b the maximum numerical value of p_L tends to occur at

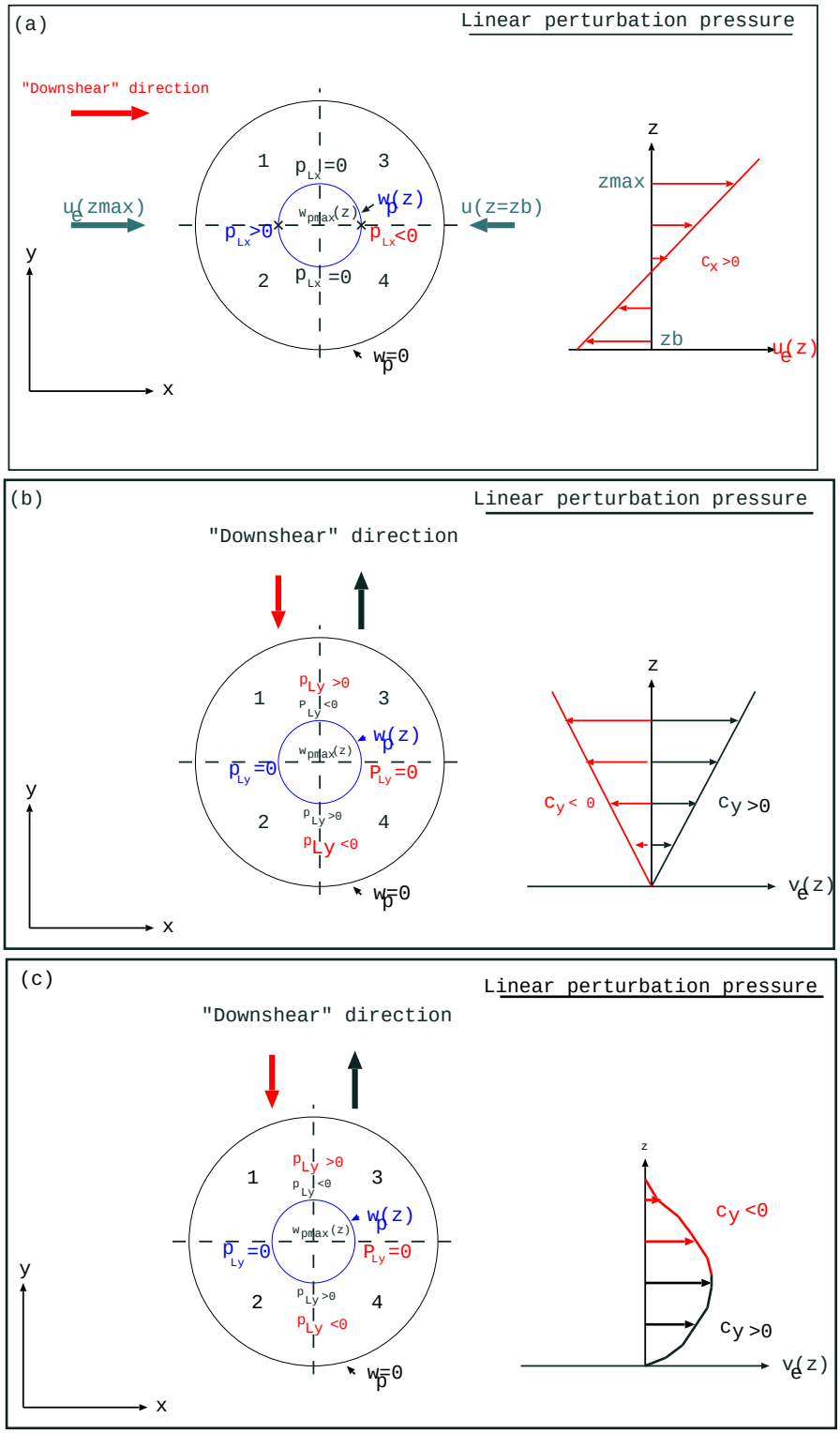

Figure 1: Qualitative distribution of linear perturbation pressure in an idealized, circular symmetric, updraft. Top, for a unidirectional constant (positive) vertical wind shear along the x-axis. Middle, for a positive (black) and negative (red) constant unidirectional vertical shear along the y-axis and bottom, for a wind profile that is a combination of of the profiles in the middle figure. See text for further explanation.

level z_{max}, at the intersection of the inner (blue) circle with the vertical dashed line (left half of Figure 1b). A downward directed vertical perturbation pressure gradient force is created below z_{max} on the upshear side of the updraft and a corresponding upward directed pressure gradient force is created on the downshear side of the updraft. The linear perturbation pressure may therefore trigger development of new cells on the downshear side and prevent development of new cells on the upshear side. With a positive u_E, constant with height, p_L *may trigger growth of new cells on the right flank of the original cell in an environment with warm advection. In an environment with cold advection* p_L *may trigger growth of new cells on the left flank of the original cell*.

A case of particular interest occurs if the v_e-profile is as depicted in Figure 1c. Such a v_e-profile can be obtained in an environment with warm advection and a significant equivalent barotropic component of the thermal wind, giving a u_e-profile like the one in Figure 1a. If the v_e-profile in Figure 1c represents conditions in the environment below the level z_{max} of maximum updraft velocity, the linear perturbation pressure is zero at the level z_*, of maximum v_e, located below z_{maz}. Below z_*, p_L is negative and positive on the left and right flank of the updraft, respectively (when looking in the positive x-direction). Above z_* the opposite is the case: p_L is positive and negative on the left and right flank of the updraft, respectively. A case like the one depicted in Figure 1c combined with a u_e-profile as in Figure 1a therefore may have a potential for larger vertical gradients of the linear perturbation pressure, meaning a higher probability of generating organized severe convection (multicell storms), than cases with v_e-profiles as in Figure 1b.

A majority of multicell storms are observed in an environment with warm advection. In cold advection the amount of CAPE in the environment usually is relatively small. The conditions for development of organized severe convection is therefore usually less favorable in cold advection.

It is left as an exercise to discuss the linear perturbation pressure connected with downdrafts.

Effect of nonlinear perturbation pressure

The nonlinear perturbation pressure p_{NL} is given approximately by (24). The vertical component of the perturbation vorticity $\vec{\zeta_p}$ is likely to give a significant contribution to p_{NL} in an environment with a strong vertical shear of the horizontal wind, since generation of ζ_{pz} involves interaction between the flow in the environment and the vertical perturbation velocity w_p. The interaction takes place through the twisting or tilting term in the vorticity equation for ζ_{pz}. The contribution from the twisting term to the rate of change with time of ζ_{pz} is given by (26). The vorticity in the environment is by definition

$$\begin{aligned}\vec{\zeta_e} &= \left(\frac{\partial w_e}{\partial y} - \frac{\partial v_e}{\partial z}\right)\vec{i} + \left(\frac{\partial u_e}{\partial z} - \frac{\partial w_e}{\partial x}\right)\vec{j} + \left(\frac{\partial v_e}{\partial x} - \frac{\partial u_e}{\partial y}\right)\vec{k} \\ &= -\frac{\partial v_e}{\partial z}\vec{i} + \frac{\partial u_e}{\partial z}\vec{j} + \left(\frac{\partial v_e}{\partial x} - \frac{\partial u_e}{\partial y}\right)\vec{k}, \end{aligned} \tag{6}$$

where the last equality follows from the approximation $w \approx w_p$, based on the observation that $|w_e| << |w_p|$ in an environmrnt with deep convection. Equation (3) can therefore be written

$$\left(\frac{\partial \zeta_{pz}}{\partial t}\right)_{twist} = \zeta_{ey}\frac{\partial w_p}{\partial y} + \zeta_{ex}\frac{\partial w_p}{\partial x}, \tag{7}$$

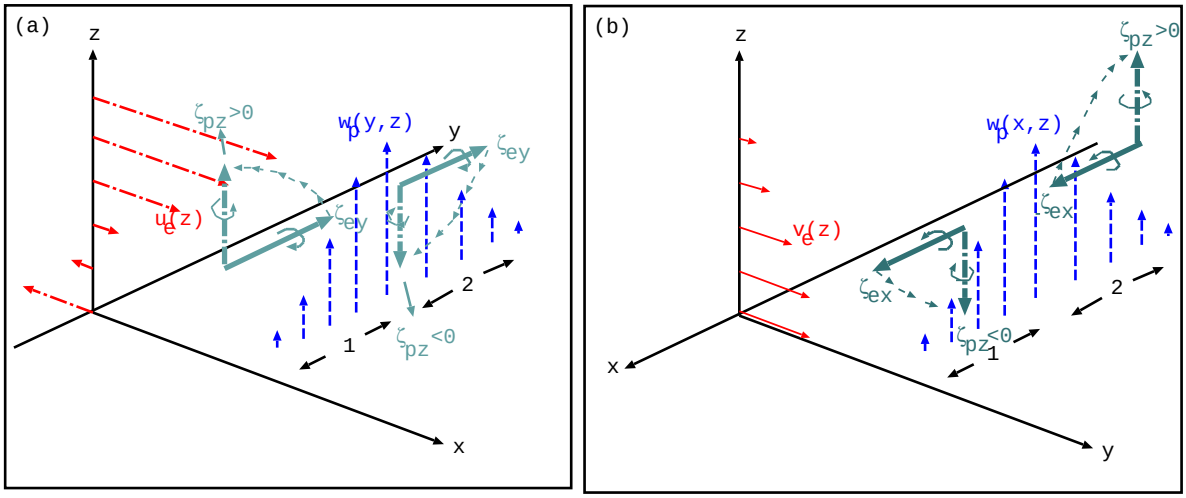

Figure 2: Qualitative distribution of non-linear perturbation pressure, created by twisting of perturbation vorticity in the vertical plane by the environmental wind in an idealized, circular symmetric, updraft. Left (a), for a constant (positive) unidirectional vertical shear along the x-axis and right (b), for a constant (negative) unidirectional vertical shear along the y-axis. See text for further explanation.

showing more clearly how horizontal vorticity in the environment interacts with the vertical perturbation velocity to create perturbation vorticity along the vertical axis. Generation of ζ_{pz} by twisting of $\vec{\zeta}_e$ in the vertical plane by w_p is shown schematically in Figure 2. Figure 2a illustrates twisting of ζ_{ey}, the component of horizontal vorticity in the environment along the y-axis, due to variation of w_p in the same direction. Similarly, Figure 2b shows twisting of ζ_{ex}, the component of environmental vorticity along the x-axis, due to variation of w_p in the same direction. According to (7) the rule in a region of updraft is that *positive (cyclonic) and negative (anticyclonic)* ζ_{pz} *is generated on the right and left flank of the updraft when looking downshear*, i.e. in Figure 2a in the positive x-direction and in Figure 2b in the negative y-direction. Equivalently, the rule can be formulated as follows:*when looking in the direction perpendicular and to the right of the horizontal vorticity vector in the environment, cyclonic and anticyclonic* ζ_{pz} *is generated on the right and left flank of the updraft, respectively*.

Close to a level ground or water surface both w_p and $\nabla_z w_p$ are small, implying no or weak generation of ζ_{pz} and no or weakly negative nonlinear perturbation pressure p_{NL}. Since $\nabla_z w_p$ tends to increase with increasing updraft velocity, generation of ζ_{pz} tends to increase with height and according to (2) the associated p_{NL} tends to become more negative with height. If the vertical shear of the the environmental velocity is constant (as in Figure 2) $|\zeta_{pz}|$ tends to have a maximum and p_{NL} the largest negative value at the level z_{max} of maximum updraft velocity. For environmental vorticity aligned with the y-axis, p_{NL} tends to become a (negative) minimum and $|\zeta_{pz}|$ a maximum at the intersections of the inner (blue) circle and the vertical dashed line in the idealized case shown in Figure 1a. Likewise, for environmental vorticity aligned with the x-axis the extreme values of p_{NL} and $|\zeta_{pz}|$ tend to occur at the intersections of the blue circle with the horizontal dashed line.

Due to the negative nonlinear perturbation pressure associated with perturbation vorticity along the vertical axis, air is accelerated upward by a negative $\partial p_{NL}/\partial z$ below z_{max} on both the right and left side of the updraft (when looking downshear or equivalently, in the direction perpendicular and to the right of the horizontal vorticity vector in the environment). Conditions may become favorable for development of new cells on both sides of the original cell. This process is called *storm splitting* and

has been observed in North America and documented by Burgess, 1974. Note that the growing cells are rotating, anticyclonically to the left and cyclonically to the right relative to the downshear direction (Figure 2). The rotating updrafts are called mesocyclones. They are typical for supercell storms. Like multicell storms, super-cell storms usually form in an environment characterized by warm advection. Since the linear perturbation pressure tends to suppress growth of new cells on the downshear left side of updrafts, new cells tends only to develop on the downshear right side of updrafts. For this reason mainly, supercell storms are often observed to propagate to the right of the direction of movement of individual cells. This relatively common type of storms (including multicell storms) are called *right moving* storms or *right movers* (see for example Browning, 1964).

It is again left as an exercise to discuss the p_{NL} pattern due to downdrafts.

A multicell storm case over Northern Germany

Most cases of organized severe convection, documented in the literature, are from the United States. However, it does not mean that this type of convection is uncommon in other parts of the World. In Europe, for example, organized severe convection occurs every year with a maximum frequency in the late Spring to early Autumn period. Multicell storms in Europa may form as far north as in Finland.

In this section a case study of a multicell storm development over the southeast North Sea and Northern Germany will be briefly presented. The event took place in the morning on 9 June 2004. The synoptic-scale conditions are shown in Figure 3. Shown in the upper row of this figure is water vapor images (channel 6) from the first Meteosat Second Generation (MSG) geostationary satellite at 00 UTC (left) and 06 UTC (right). The images show an eastward moving large-scale ridge over Western Europe. This large-scale wave is also shown by the wind field at 300 hPa (Figure 3, lower left) and in the 300 hPa relative vorticity (Figure 3, lower right). On the MSG images there is indication of a superposed southeast-ward moving short-wave trough downstream of the large-scale ridge. At 06 UTC the short-wave perturbation has formed a convex cloud edge towards drier air over the southwestern Sweden and the Baltic proper (Figure 3, upper right). In the relative vorticity pattern (Figure 3, lower right) the short-wave trough can be seen as a comma-shaped band of positive (cyclonic) relative vorticity from Jutland to the southeastern North Sea. Downstream of the short-wave trough positive relative vorticity advection becoming more cyclonic with height tends to force upward motion over Northern Germany. Figure 4 (bottom) shows that the same region has warm advection (shown by the veering with height of the horizontal wind) in the lower troposphere, which also tend to force upward motion. In addition frontal circulation forces upward motion on the warm side of the frontal zone shown in Figure 4 (top). In the latter figure the frontal zone (in terms of equivalent potential temperature (θ_e)) is seen to slope towards the colder and drier air mass to the left (marked with grey colors in the figure). At 06 UTC the surface front in the cross section is located near 54 N, 8 E (see also Figure 4, bottom). Presence of potential instability on the warm side of the front is indicated by a low-level maximum in θ_e.

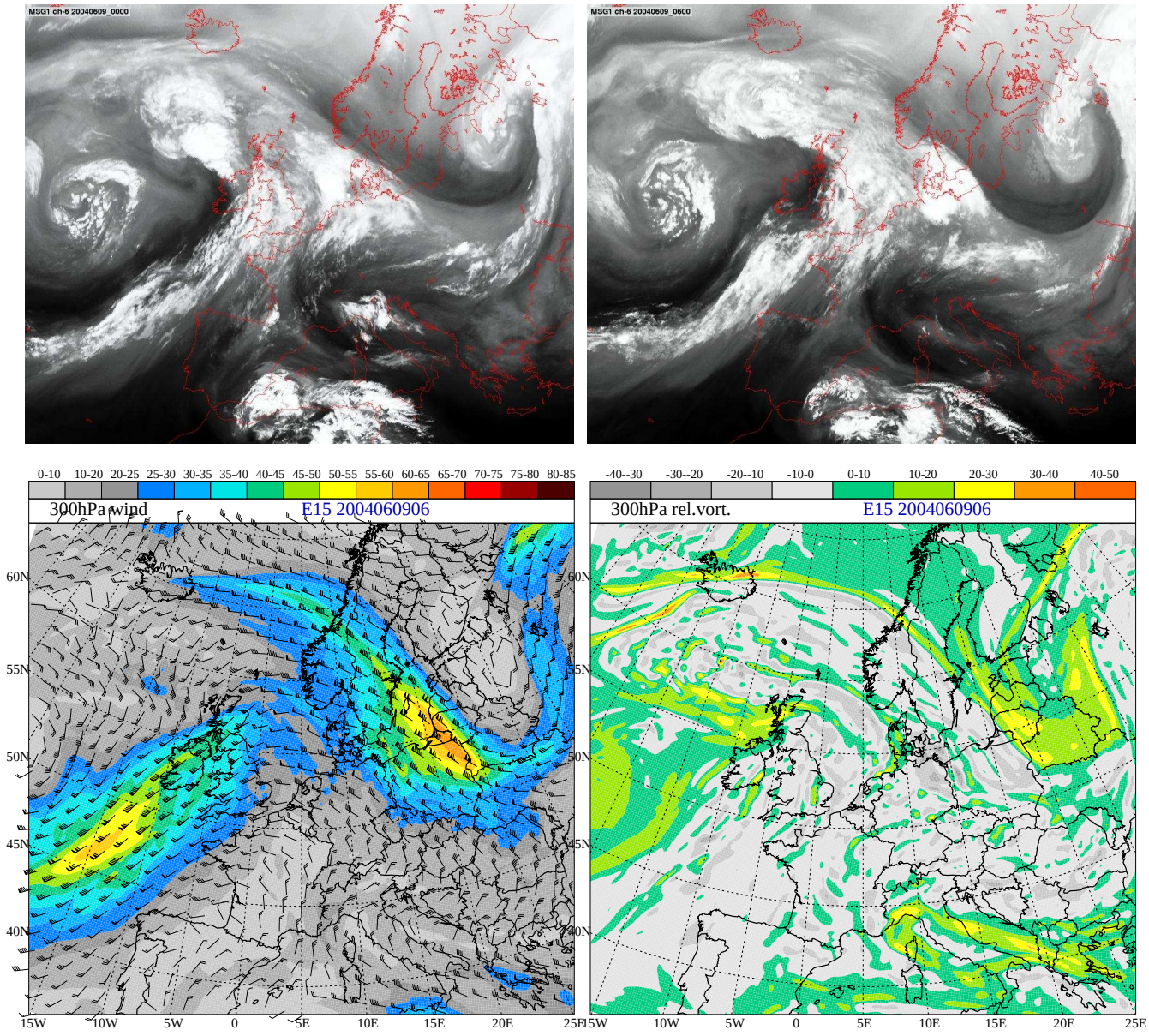

Figure 3: Top: Meteosat second generation water vapor channel 6 images at 00 UTC (left) and 06 UTC (right) on 9 June 2004. Bottom: Analyzed wind velocity at 300 hPa with color scale in $m\,s^{-1}$ (left) and analyzed relative vorticity at 300 hPa with color scale (grey for anticyclonic and green to yellow for cyclonic vorticity) in units $10^{-5}\,\mathrm{s}^{-1}$ (right) at 06 UTC on 9 June 2004.

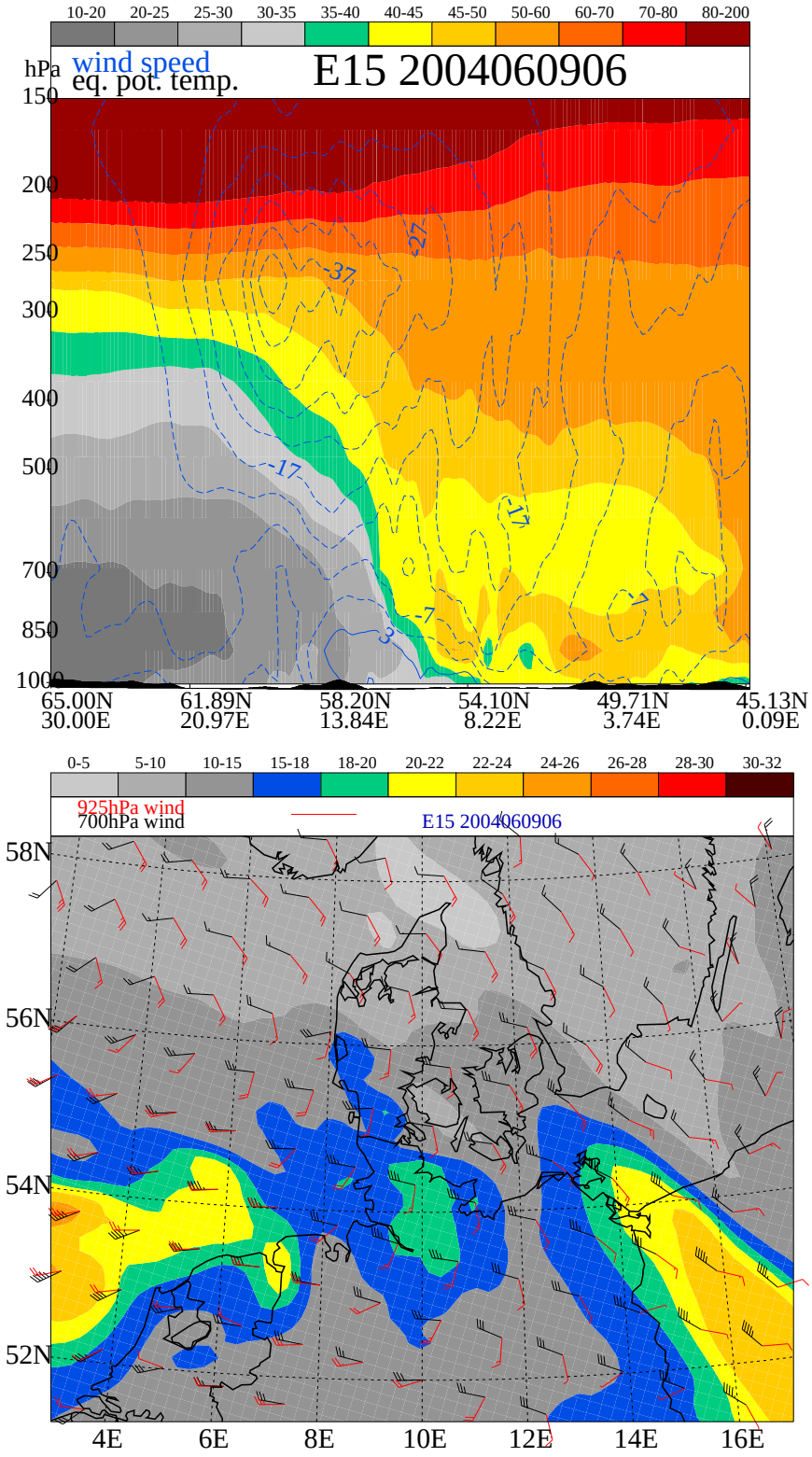

Figure 4: Top: Vertical cross section, approximately perpendicular to the warm front over Northern Germany, showing wind speed normal to the cross section in $\mathrm{m\,s^{-1}}$ (dashed blue curves) and equivalent potential temperature with color scale in K. Bottom: Wind at 925 hPa (red barbs) and at 700 hPa (black barbs) with color scale in $\mathrm{m\,s^{-1}}$ for wind at 700 hPa. Analysis time: 6 UTC on 9 June 2004.

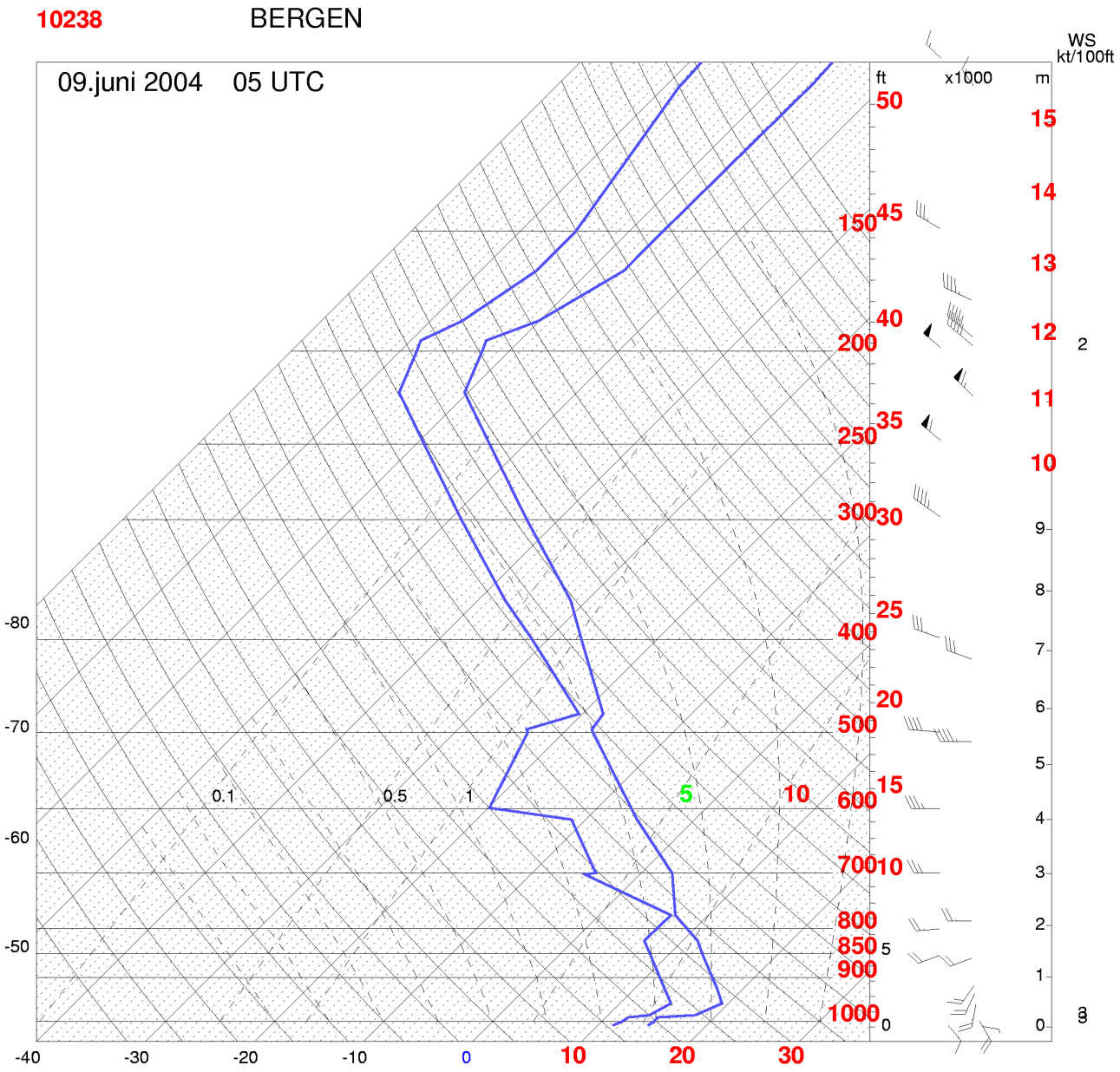

Figure 5: Sounding from Bergen at position 52.81 N, 9.93 E (Northern Germany) at 05 UTC on 9 June 2004.

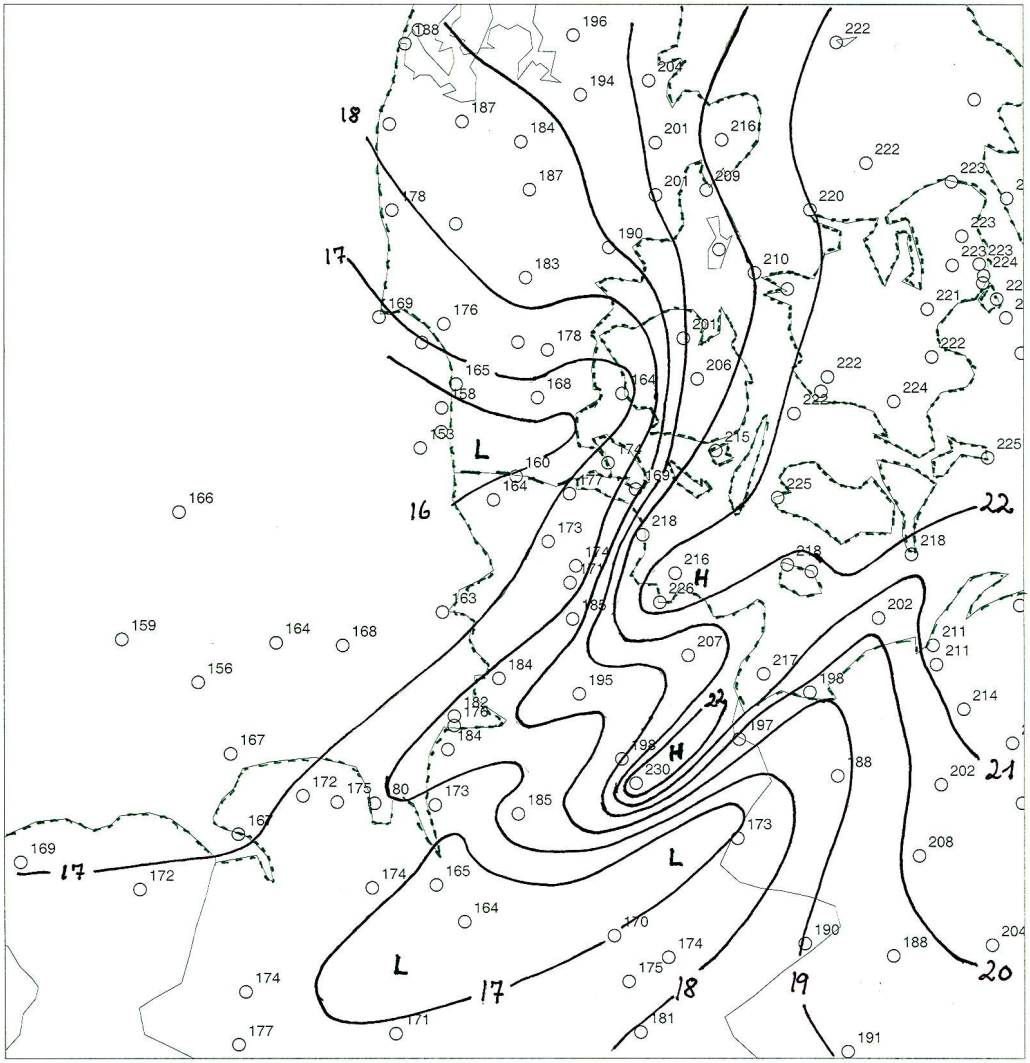

Figure 6: Subjective analysis of mean sea level pressure (interval 1 hPa) at 06 UTC on 9 June 2004.

The sounding in Figure 5 is believed to be representative for the relatively warm and moist air mass (marked by green, yellow and red colors in Figure 4). The sounding has a potential unstable layer above 780 hPa. The shallow, stably stratified layer at the surface is likely to be a nocturnal surface inversion or cool air originating from nearby downdrafts. The sounding indicates that the air at the top of the surface inversion is conditionally unstable with a lifting condensation level (LCL) around 900 hPa, a level of free convection (LFC) near 800 hPa and an equilibrium level (EL) near the tropopause at approximately 220 hPa. The EL (for an undiluted parcel ascent) is the level above LFC where the temperature in the ascending parcel becomes equal to the sounding temperature. The convective available potential energy (CAPE) for the near-surface air is proportional to the positive area between the temperature curve for the ascending parcel (above LFC approximately a pseudo adiabat, since θ_e is approximately conserved) and the temperature curve of the sounding. The sounding shows a moderately high value of CAPE for air on top of the surface inversion.

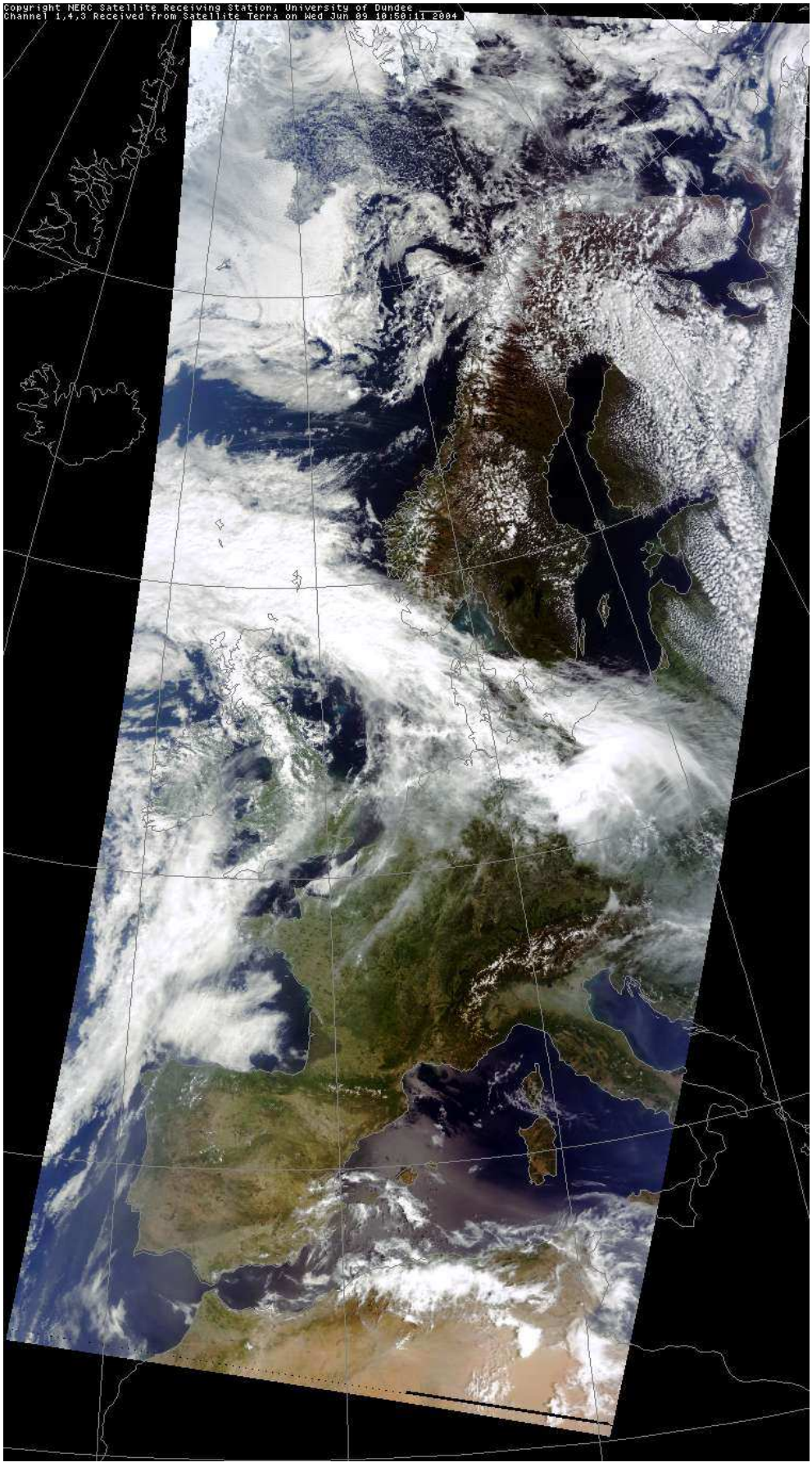

Figure 7: Satellite Terra image, channel 1,4,3, 10.50 UTC on 9 June 2004. Courtesy Dundee Satellite Receiving Station (www.sat.dundee.ac.uk]

The variation with hight of the horizontal wind in the environment is shown to the right in Figure 5. Note that there is warm advection throughout the troposphere, since the wind veers with hight from the surface to the tropopause.

Imagine that the positive x-axis points towards southeast. Then the wind profile $u_e(z)$ along the x-axis becomes comparable to the u_e-profile in Figure 1 and 2 and the wind-profile $v_e(z)$ along the y-axis becomes comparable to the v_e-profile in Figure 1, bottom. This indicates that conditions for development of right moving multicell storms are present downstream of the upper level short-wave trough, particularly in the region with forced ascent due to warm front circulation, differential relative vorticity advection becoming more cyclonic with height and warm advection. The moderately high CAPE and strong vertical shear (approximately $5 \cdot 10^{-3}\ \mathrm{s}^{-1}$) in the sounding at 05 UTC(Figure 5) does not exclude the possibility for development of right moving supercell storms. Numerous reports of severe weather (heavy rain, severe gusty winds and abundant lightening) along the track of the upper-tropospheric short-wave trough exist, but to the authors knowledge no reports of mesocyclones (cyclonically rotating updrafts) have been given. The latter might indicate (but does not prove) that no supercell storms formed during the organized severe convection event in the morning on June 9 2004. The severity and organized nature of the event is also indicated by the mean sea level pressure (mslp) analysis in Figure 6. According to this figure at least one squall line has formed over Northern Germany at 06 UTC. Note the abrupt rise in mslp behind the squall line. Figure 7 shows that the convective system by 10.50 UTC has moved southeastward to the boarder between Germany and Poland. At this time the system apparently covers an area comparable in size with Jutland.

Appendix: The background and perturbation states

Due to the high Rossby number (Ro) in severe convection the frictionless momentum equation valid for this situation can be approximated by

$$\frac{D\vec{V}}{Dt} = -\frac{1}{\rho}\nabla p - g\vec{k}. \tag{8}$$

Note that the Coriolis acceleration has been omitted in (8), since it is one order of magnitude smaller than the acceleration on the left hand side (lhs), where the operator
$D/Dt = \partial/\partial t + \vec{V}\cdot\nabla = \partial/\partial t + u\cdot\partial/\partial x + v\cdot\partial/\partial y + w\cdot\partial/\partial z$.

In (8) $\vec{V} = u\vec{i} + v\vec{j} + w\vec{k}$ is the velocity (measured relative to a storm system moving with constant velocity), $\nabla p = \partial p/\partial x\vec{i} + \partial p/\partial y\vec{j} + \partial p/\partial z\vec{k}$ is the pressure gradient, ρ is density and g is gravity (treated as constant). The unit vectors $\vec{i}$, $\vec{j}$ and $\vec{k}$ point along the three orthogonal directions in space.

Convection can be considered as a perturbation to a background or environmental state. For convenience the background state is defined such that it is horizontally homogeneous and time independent. Furthermore, the background is in hydrostatic balance. This means that the background state has $\vec{V_e} = u_e(z)\vec{i} + v_e(z)\vec{j} + w_e(z)\vec{k}$ and the thermodynamic variables $p_e(z), \rho_e(z)$ and $T_e(z)$ for the environmental state are related by the hydrostatic equation

$$\frac{\partial p_e}{\partial z} = -g\rho_e \tag{9}$$

and the equation of state for an ideal gas

$$T_e = \frac{p_e}{R\rho_e}. \tag{10}$$

The perturbed (convective) part of the state has $\vec{V_p} = u_p\vec{i} + v_p\vec{j} + w_p\vec{k} = (u-u_e)\vec{i} + (v-v_e)\vec{j} + (w-w_e)\vec{k}, p_p = p - p_e, \rho_p = \rho - \rho_e$ and $T_p = T - T_e$, where all the perturbation variables (denoted by subscript p) are functions of x, y, z and t (time).

Since the vertical velocity, w_e, in the environment is small (order of $10^{-2}\,\mathrm{m\,s^{-1}}$) and w_p is of order $10\ \mathrm{ms}^{-1}$ it can be assumed (for simplicity) that $w_e = 0$.

Since $|\rho_p/\rho_e| \sim |T_p/T_e| << 1$, equation (8) can be approximated further to

$$\frac{D\vec{V}}{Dt} = -\frac{1}{\rho_e}\nabla p_p + B\vec{k}, \tag{11}$$

where $B = -\rho_p/\rho_e g$ is the buoyancy of the perturbed air. Taking the 3-dimensional divergence ($\nabla\cdot$) of (11) yields

$$\nabla\cdot\frac{D\vec{V}}{Dt} = -\nabla\cdot({\rho_e}^{-1}\nabla p_p) + \frac{\partial B}{\partial z}. \tag{12}$$

It is left as an exercise to show that

$$\nabla\cdot\frac{D\vec{V}}{Dt} = \frac{D}{Dt}\nabla\cdot\vec{V} + \nabla\vec{V}\cdot\nabla\vec{V} + \frac{1}{2}(\vec{\epsilon}\cdot\vec{\epsilon} - \vec{\zeta}\cdot\vec{\zeta}). \tag{13}$$

In(13) $\nabla\vec{V} = \partial u/\partial x\vec{i} + \partial v/\partial y\vec{j} + \partial w/\partial z\vec{k}$ is the gradient of the velocity and $\vec{\epsilon}\cdot\vec{\epsilon}$ and $\vec{\zeta}\cdot\vec{\zeta}$ are the square magnitudes of the deformation vector $\vec{\epsilon}$ and the vorticity vector $\vec{\zeta}$, respectively. The deformation vector, $\vec{\epsilon}$, is defined as

$$\vec{\epsilon} = (\frac{\partial w}{\partial y} + \frac{\partial v}{\partial z})\vec{i} + (\frac{\partial u}{\partial z} + \frac{\partial w}{\partial x})\vec{j} + (\frac{\partial v}{\partial x} + \frac{\partial u}{\partial y})\vec{k} \tag{14}$$

and the vorticity vector, $\vec{\zeta}$, is defined as

$$\vec{\zeta} = (\frac{\partial w}{\partial y} - \frac{\partial v}{\partial z})\vec{i} + (\frac{\partial u}{\partial z} - \frac{\partial w}{\partial x})\vec{j} + (\frac{\partial v}{\partial x} - \frac{\partial u}{\partial y})\vec{k} \tag{15}$$

Substitution of (13) into (12), rearrangement of terms and utilizing the mass continuity equation to replace $\nabla\cdot\vec{V}$ with $-\rho^{-1}D\rho/Dt$ leads to

$$-\frac{D}{Dt}\left(\frac{D\ln\rho}{Dt}\right) + {\rho_e}^{-1}\left(\nabla^2 p_p - \frac{\partial\ln\rho_e}{\partial z}\frac{\partial p_p}{\partial z}\right) = -\nabla\vec{V_p}\cdot\nabla\vec{V_p} - \frac{1}{2}(\vec{\epsilon}\cdot\vec{\epsilon} - \vec{\zeta}\cdot\vec{\zeta}) + \frac{\partial B}{\partial z}. \tag{16}$$

A scale analysis indicates that the terms on the lhs of (16) containing $\ln \rho$ (or $\ln \rho_e$) tends to be an order of magnitude smaller than the other terms in the equation. For further qualitative discussions (16) can therefore be simplified to

$$\rho_e{}^{-1}\nabla^2 p_p = -\nabla\vec{V_p}\cdot\nabla\vec{V_p} - \frac{1}{2}\left(\vec{\epsilon}\cdot\vec{\epsilon} - \vec{\zeta}\cdot\vec{\zeta}\right) + \frac{\partial B}{\partial z}. \tag{17}$$

This is a diagnostic equation for the perturbation pressure p_p, showing how it responds to the forcing terms on the right hand side (rhs). The forcing terms are: the vertical gradient of the buoyancy and terms proportional to the square magnitudes of the deformation, relative vorticity and velocity gradient vectors.

By definition $\vec{\epsilon} = \vec{\epsilon_e} + \vec{\epsilon_p}$ and $\vec{\zeta} = \vec{\zeta_e} + \vec{\zeta_p}$. Hence,

$$\begin{aligned}\rho_e{}^{-1}\nabla^2 p_p = {} & \frac{\partial B}{\partial z} - \nabla\vec{V_p}\cdot\nabla\vec{V_p} \\ & -\frac{1}{2}\left(\vec{\epsilon_e}\cdot\vec{\epsilon_e} - \vec{\zeta_e}\cdot\vec{\zeta_e} + 2(\vec{\epsilon_e}\cdot\vec{\epsilon_p} - \vec{\zeta_e}\cdot\vec{\zeta_p}) + (\vec{\epsilon_p}\cdot\vec{\epsilon_p} - \vec{\zeta_p}\cdot\vec{\zeta_p})\right).\end{aligned} \tag{18}$$

Since $\vec{\epsilon_e}\cdot\vec{\epsilon_e} - \vec{\zeta_e}\cdot\vec{\zeta_e} = 0$ and $\vec{\epsilon_e}\cdot\vec{\epsilon_p} - \vec{\zeta_e}\cdot\vec{\zeta_p} = 2\partial\vec{V_e}/\partial z\cdot\nabla_z w_p$, (18) can be rewritten as

$$\nabla^2 p_p = \rho_e\left(\frac{\partial B}{\partial z} - \nabla\vec{V_p}\cdot\nabla\vec{V_p} - 2\frac{\partial\vec{V_e}}{\partial z}\cdot\nabla_z w_p - \frac{1}{2}(\vec{\epsilon_p}\cdot\vec{\epsilon_p} - \vec{\zeta_p}\cdot\vec{\zeta_p})\right). \tag{19}$$

The second, third and fourth term on the rhs of (19) is called the 'fluid extension', the 'linear' and the 'shear' term, respectively. The 'fluid extension' and 'shear' terms are nonlinear, whereas the other two terms ('linear' and 'vertical gradient of buoyancy') are linear.

Since ∇^2 is linear the perturbation pressure is the sum of contributions from each of the forcing terms on the rhs of (19). If the contributions from the buoyancy and linear and nonlinear forcing terms are denoted p_B, p_L and p_{NL}, respectively (for convenience, the subscript p has been omitted) the linearity of ∇^2 yields

$$\nabla^2 p_L = -2\rho_e\frac{\partial\vec{V_e}}{\partial z}\cdot\nabla_z w_p, \tag{20}$$

$$\nabla^2 p_{NL} = \rho_e\left(-\nabla\vec{V_p}\cdot\nabla\vec{V_p} - \frac{1}{2}(\vec{\epsilon_p}\cdot\vec{\epsilon_p} - \vec{\zeta_p}\cdot\vec{\zeta_p})\right), \tag{21}$$

and

$$\nabla^2 p_B = \rho_e\frac{\partial B}{\partial z}. \tag{22}$$

The Laplacian of a wellbehaved variable is roughly proportional to minus the variable itself. Hence, for qualitative discussions it is practical to utilize the simplified (proportional to) equations

$$p_L \sim 2\rho_e \frac{\partial \vec{V_e}}{\partial z} \cdot \nabla_z w_p, \tag{23}$$

$$p_{NL} \sim \rho_e \left(\nabla \vec{V_p} \cdot \nabla \vec{V_p} + \frac{1}{2}(\vec{\epsilon_p} \cdot \vec{\epsilon_p} - \vec{\zeta_p} \cdot \vec{\zeta_p}) \right), \tag{24}$$

$$p_B \sim -\rho_e \frac{\partial B}{\partial z}. \tag{25}$$

Equation (25) shows that p_B tends to be positive and negative above and below a maximum in buoyancy, respectively. This generates a vertical perturbation pressure gradient in opposite direction of buoyancy. In other words, the vertical perturbation pressure gradient associated with buoyancy acts to reduce the acceleration due to buoyancy.

According to (24) the 'fluid extension' term ($\rho_e \nabla \vec{V_p} \cdot \nabla \vec{V_p}$) and the deformation part of the 'shear' term ($1/2\rho_e \vec{\epsilon_p} \cdot \vec{\epsilon_p}$) tends to be associated with a positive perturbation pressure p_{NL}, whereas the relative vorticity perturbation part of the 'shear' term ($-1/2\vec{\zeta_p} \cdot \vec{\zeta_p}$) tends to be associated with a negative perturbation pressure p_{NL}.

Twisting of relative perturbation vorticity by the perturbation flow generally generates perturbation vorticity along all space directions. Twisting of environmental vorticity by the perturbation flow can generate perturbation vorticity along the vertical axis since $\vec{\zeta_e} = -\partial v_e/\partial z \vec{i} + \partial u_e/\partial z \vec{j}$ and the generation of vertical perturbation vorticity, $\zeta_{pz} = \vec{k} \cdot \vec{\zeta_p} = \partial v_p/\partial x - \partial u_p/\partial y$, is

$$\left.\frac{\partial \zeta_{pz}}{\partial t}\right|_{twist} = \vec{k} \cdot \frac{\partial \vec{V_e}}{\partial z} \times \nabla_z w_p = \frac{\partial u_e}{\partial z}\frac{\partial w_p}{\partial y} - \frac{\partial v_e}{\partial z}\frac{\partial w_p}{\partial x}. \tag{26}$$

As described in previous sections the perturbation pressure generated by interaction between the environmental flow ($\vec{V_e}$) and the perturbation flow (primarily w_p) associated with convection may have an important influence on how the convection evolves with time. The influence is primarily through the linear perturbation pressure P_L from (23) and the nonlinear perturbation pressure P_{NL} from (26) and (24).

Theoretical work on organized, severe convection can be found in for example Rotunno, 1981; Rotunno and Klemp, 1982a; Rotunno and Klemp, 1982b and Rotunno et al., 1988.

Numerical simulation of organized severe convection are presented in for example Weisman and Klemp, 1982; Wilhelmson and Chen, 1982 and Weismann and Klemp, 1984.

References

[H. B. Bluestein 1993] Synoptic-Dynamic Meteorology in Midlatitudes. Vol. 2: Observations and Theory of weather systems. Oxford University Press, pp. 463-468.

[K. A. Browning 1964] Airflow and precipitation trajectories within severe local storms which travel to the right of the winds. J. Atmos. Sci., 21, 634-639.

[D. Burgess 1974] Study of a right-moving thunderstorm utilizing new single Doppler evidence. M.S. Thesis, Dept. of Meteorology, Univ. of Oklahoma, Norman.

[R. Rotunno 1981] On the evolution of thunderstorm rotation. Mon. Wea. Rev., 109, 577-586.

[R. Rotunno and J. B. Klemp 1982a] The influence of shear-induced pressure gradient on thunderstorm motion. Mon. Wea. Rev., 110, 136-151.

[R. Rotunno and J. B. Klemp 1982b] On the rotation and propagation of simulated supercell thunderstorms. J. Atmos. Sci., 42, 271-292.

[R. Rotunno, J. B. Klemp, and M. L. Weismann 1988] A theory for strong, long-lived squall lines. J. Atmos. Sci., 45, 463-485.

[M. L. Weismann and J. B. Klemp 1982] The dependence of numerically simulated convective storms on vertical wind shear and buoyancy. Mon. Wea. Rev., 110, 504-520.

[M. L. Weismann and J. B. Klemp 1984] The structure and classification of numerically simulated convection storms in directionally varying wind shears. Mon. Wea. Rev., 112, 2479-2498.

[R. B. Wilhelmson and C.-S. Chen 1982] A simulation of the development of successive cells along a cold outflow boundary. J. Atmos. Sci., 139, 1466-1483.

Previous reports

Previous reports from the Danish Meteorological Institute can be found at:
http://www.dmi.dk/dmi/dmi-publikationer.htm